ACS APPLIED MATERIALS & INTERFACES

Research Article

www.acsami.org

Efficient Enrichment and Self-Assembly of Hybrid Nanoparticles into Removable and Magnetic SERS Substrates for Sensitive Detection of Environmental Pollutants

Siying Tang,[†,∥] Yong Li,[†,∥] Hao Huang,[†] Penghui Li,[*,†,‡] Zhinan Guo,[†,§] Qian Luo,[*,†] Zhe Wang,[†] Paul K. Chu,[‡] Jia Li,[†] and Xue-Feng Yu[*,†]

[†]Institute of Biomedicine and Biotechnology, Shenzhen Institutes of Advanced Technology, Chinese Academy of Sciences, Shenzhen 518055, P. R. China

[‡]Department of Physics and Materials Science, City University of Hong Kong, Tat Chee Avenue, Kowloon, Hong Kong, P.R. China

[§]SZU-NUS Collaborative Innovation Center for Optoelectronic Science and Technology, and Key Laboratory of Optoelectronic Devices and Systems of Ministry of Education and Guangdong Province, College of Optoelectronic Engineering, Shenzhen University, Shenzhen 518060, P. R. China

Supporting Information

ABSTRACT: A structure consisting of a low surface energy substrate and low surface tension liquid is designed and prepared by taking advantage of perfluorinated fluid infusion into the porous Teflon membrane. This slippery platform allows efficient enrichment and self-assembly of hybrid nanoparticles and the assembled structure can be detached from the membrane. A macroscale superlattice array of Au nanorods doped with magnetic Fe_3O_4 nanoparticles is obtained by suppressing the outward capillary flow and coffee-ring effect during evaporative self-assembly. In SERS (surface enhanced Raman scattering) detection of environmental pollutants including thiram, diquat and polycyclic aromatic hydrocarbons, the removable plasmonic superlattice array with magnetic properties enables rapid separation of analytes from the solution resulting in excellent sensitivity and detection limits down to the nanomolar level. The self-assembly strategy shows great potential in the fabrication of removable 3D plasmonic superlattice arrays for SERS detections.

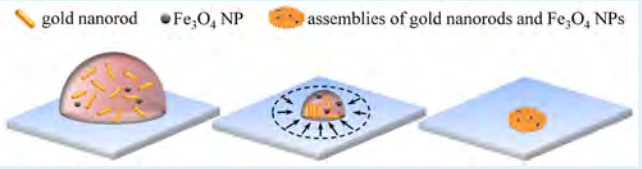

KEYWORDS: *evaporative self-assembly, surface enhanced Raman scattering, gold nanorods, surface modification, environmental pollutants*

1. INTRODUCTION

Surface enhanced Raman scattering (SERS) has recently emerged as one of the mainstream spectroscopic methods and been adopted in various analytical fields. SERS is attractive due to its capability to provide a spectroscopic fingerprint of each type of molecule providing label-free and rapid on-site detection of different analytes.[1−5] Although ultrasensitive analysis can be carried out with SERS by taking advantage of the electromagnetic enhancement of noble metal nanostructures, application to molecular analysis is plagued by problems associated with the reproducibility and complexity in substrate preparation. In practice, analytes such as environmental pollutants always exist in complex samples at low concentrations and need to be effectively captured by the SERS substrate and separated from the complex external medium. Hence, the requirements for the desirable SERS substrate are efficient enhancement of the Raman signals and easy separation from the complex solutions.

SERS signals arise from plasmon resonance on the surface of metallic nanostructures and there have been extensive efforts to generate metallic nanostructures with sub-10 nm narrow gaps for efficient plasmon resonance.[6−9] Recently, the droplet evaporative self-assembly technique has been proposed as a green approach to construct superlattice nanostructures as SERS substrates by assembling the metal nanoparticle building blocks available from wet-chemical synthesis.[10−15] Compared to traditional physical nanofabrication techniques, the chemical self-assembly method which does not require extensive instrumentation is economical boding well for mass production of SERS substrates comprising different metallic nanoparticles (NPs). However, since evaporation of a sessile droplet containing insoluble NPs always produces the "coffee-ring" like stain, the big challenge concerning droplet evaporative self-assembly is dense and uniform packing of NPs.[16,17] Very recently, different strategies have been proposed to suppress the "coffee-ring" effect during self-assembly and uniform deposition of metallic NPs such as gold nanorods (AuNRs) has been demonstrated.[18−23] However, similar to traditional physical

Received: December 16, 2016
Accepted: February 9, 2017
Published: February 9, 2017

DOI: 10.1021/acsami.6b16141
ACS Appl. Mater. Interfaces 2017, 9, 7472−7480

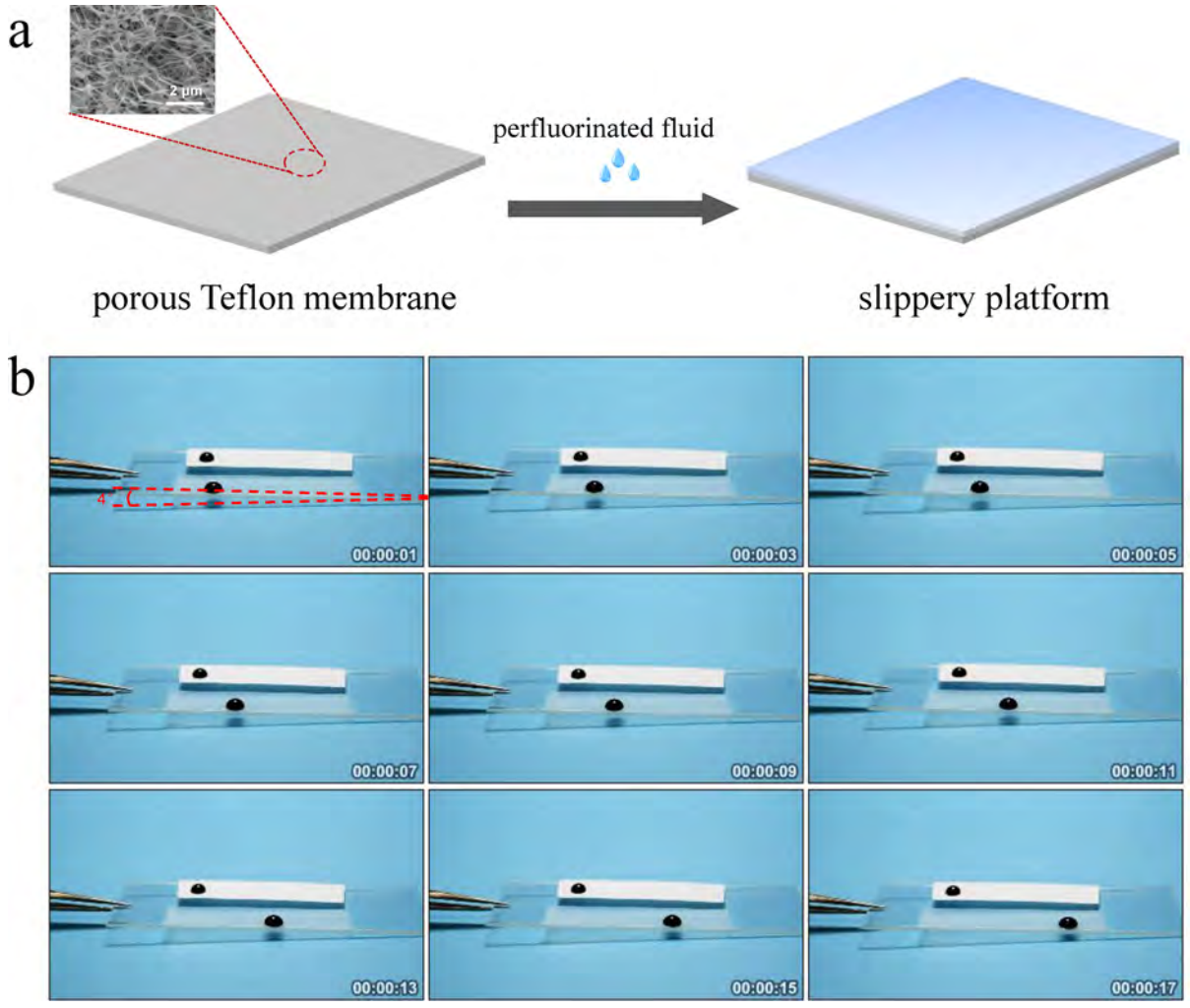

Figure 1. (a) Schematic illustration of the slippery platform with the perfluorinated fluid infusing the Teflon membrane and (b) Photographs illustrating the droplet mobility on the treated (front) and untreated (behind) Teflon membrane.

techniques, these self-assembled SERS substrates are still immobilized on the bulk base materials such as silicon chips and prone to interfering SERS signals thus stifling direct separation of the analytes from the solution. Consequently, it is desirable to prepare a removable SERS substrate allowing controlled capture and separation of analytes from the complex solutions for efficient SERS detection.

Herein, the evaporative self-assembly technique is adopted to fabricate a magnetically controllable and removable SERS substrate. By using a perfluorinated fluid to infuse the porous Teflon membrane, the slippery platform comprising a low surface energy substrate and low surface tension liquid enables efficient enrichment and self-assembly of hybrid nanoparticles to the removable macroscale structure. A superlattice array of Au nanorods doped with magnetic Fe_3O_4 nanoparticles is fabricated and used in SERS detection of environmental pollutants, the removable plasmonic superlattice array with magnetic properties allows rapid separation of analytes from the solution and yields excellent sensitivity.

2. MATERIALS AND METHODS

2.1. Materials. Chloroauric acid ($HAuCl_4 \cdot 4H_2O$, 99.99%), hexadecyltrimethylammonium bromide (CTAB, 97.0%), sodium borohydride ($NaBH_4$, 96%), silver nitrate ($AgNO_3$, 99.8%), L-ascorbic acid (AA, 99.7%), and malachite green (MG, 99%) were obtained from Sinopharm Chemical Reagent Co. Ltd. (Shanghai, China) and 11-mercaptoundecyl hexa(ethylene glycol) (MUDOL, 90%) was purchased from Sigma-Aldrich Co. Thiram, diquat, and polycyclic aromatic hydrocarbon solutions (PAHs) were acquired from AccuStandard Inc. All the chemicals were used as received without further purification and Millipore Milli-Q water (resistivity >18 MΩ cm^{-1} at 25 °C) was used in the experiments. The perfluorinated fluid (Krytox GPL 100) was purchased from DuPont and Teflon membranes with thickness of approximately 70 μm were bought from Sterlitech Corporation, WA.

2.2. Synthesis of AuNRs. The AuNRs were synthesized by the seed-mediated method in the CTAB solution. Briefly, 3−4 nm gold seed particles were prepared by mixing $HAuCl_4$ (0.5 mM, 5 mL) and CTAB (0.2 M, 5 mL). The solution was stirred vigorously and freshly prepared ice-cold $NaBH_4$ (10 mM, 600 μL) was added. After stirring for 2 min, the seed solution was stored at room temperature for further use. In the AuNRs synthesis, $HAuCl_4$ (5 mM, 18 mL) and $AgNO_3$ (0.1 M, 225 μL) were added to CTAB (0.2 M, 90 mL) and then HCl (1.2 M, 225 μL) and ascorbic acid (10 mM, 11.1 mL) were added and gently swirled as the color changed from dark orange to colorless. After the color change, the CTAB-stabilized gold seed solution (150 μL) was injected rapidly and the solution was gently mixed for 10 s and left overnight. Finally, the solution was centrifuged at 12 000 rpm for 15 min to stop the reaction. The supernatant was removed and the precipitate was resuspended in ultrapure water.

2.3. Surface Ligand Exchange of AuNRs. The freshly prepared CTAB-AuNRs suspension (5 mL) was purified by a second

DOI: 10.1021/acsami.6b16141
ACS Appl. Mater. Interfaces 2017, 9, 7472−7480

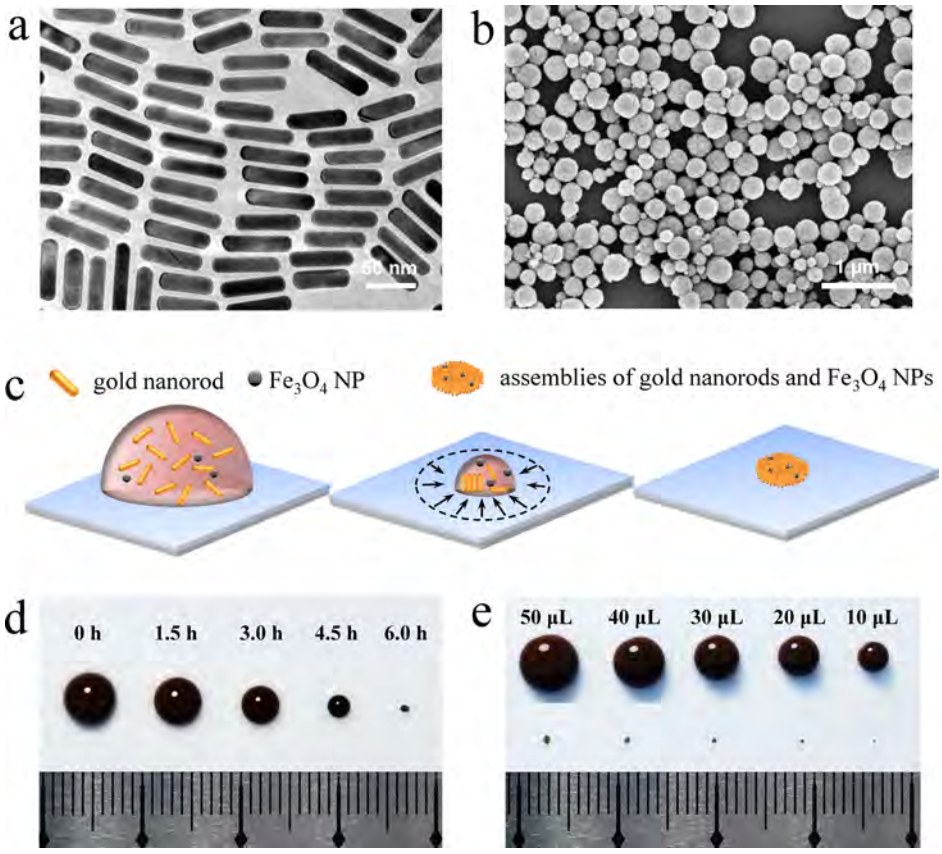

Figure 2. (a) TEM image of AuNRs; (b) SEM image of Fe_3O_4 NPs; (c) Schematic illustration of the enrichment and self-assembly of AuNRs and Fe_3O_4 hybrid NPs on the slippery platform; (d) Droplet evaporation and condensation of the 40 μL suspension of AuNRs and Fe_3O_4 hybrid NPs; (e) Droplet evaporation and condensation process of the droplet with different volumes.

centrifugation step (10 000 rpm, 10 min) to remove excess CTAB. The precipitate was dispersed in Milli-Q water (5 mL) and mixed with the MUDOL solution (0.2 mM, 5 mL). The mixture was vortexed briefly and stirred gently at room temperature for 24 h to achieve saturated adsorption of MUDOL molecules on the AuNRs. The final MUDOL-AuNRs were condensed and used in the self-assembling experiments without further purification.

2.4. Synthesis of Magnetic Fe_3O_4 Nanoparticles. In the synthesis of Fe_3O_4 nanoparticles, $FeCl_3{\cdot}6\,H_2O$ (1.64 g) and NaAc (3.6 g) were dissolved in ethylene glycol (60 mL) to form a clear solution. The mixture was stirred vigorously for 30 min and sealed in a Teflon-lined stainless-steel autoclave. The autoclave was heated to and maintained at 200 °C for 8 h and allowed to cool to room temperature afterward. The black products were separated by magnets, washed several times with ethanol, and dried under vacuum.

2.5. Self-Assembly of AuNRs and Fe_3O_4 Hybrid Nanoparticles. The slippery platform for self-assembly of AuNRs and Fe_3O_4 is fabricated by the approach inspired by *Nepenthes* pitcher plants. The as-received Teflon membranes were attached to a flat glass slide and the perfluorinated fluid (GPL 100) serving as the lubricant was sprayed onto the Teflon membranes. The lubricated sample was spun at 1000 rpm for 1 min to remove excess lubricants. The slippery platform was developed for evaporation and self-assembly of the suspension of MUDOL-AuNRs and Fe_3O_4. In a typical experiment, MUDOL-AuNRs suspension was concentrated 50 times and then mixed with Fe_3O_4 NPs suspension, and formed a hybrid suspension consists of MUDOL-AuNRs and Fe_3O_4 with concentration of 0.15 nM and 75 nM, respectively. A drop of the suspension containing MUDOL-AuNRs and Fe_3O_4 (30 μL) was dripped onto the slippery platform and kept stationary at room temperature to evaporate the water.

2.6. Characterization. The absorption spectra were acquired on a Lambda 750 UV/vis/NIR spectrophotometer (PerkinElmer) and FTIR spectra were obtained on a VERTEX 70 spectrometer (Bruker, Germany). The TEM images were taken on a JEOL-2010 transmission electron microscope (JEOL Ltd., Japan) at a voltage of 200 kV. The photos of the evaporation process were recorded with a digital camera and the 3D images were obtained on a VK-X200 3D laser scanning confocal microscope (Keyence, Japan). The SEM images were acquired on a ZEISS SUPRA 55 (Carl Zeiss, Germany) field-emission scanning electron microscopy and cross-sectional examination was made on the cleaved samples. Raman scattering was performed on a Horiba Jobin-Yvon LabRam HR VIS high-resolution confocal Raman microscope equipped with a 633 nm laser as the excitation source at room temperature. In the Raman examination, thiram, diquat, and PAHs at different concentration levels were diluted from the as-purchased high concentration standard samples. The arrays were soaked in MG, thiram, diquat, and PAHs solutions, respectively, overnight for adsorption, separated by magnets, and dried in air prior to Raman analysis.

3. RESULTS AND DISCUSSION

The slippery platform plays an important role in the enrichment and self-assembly of hybrid NPs. As shown in Figure 1a, the slippery platform is fabricated with the perfluorinated fluid GPL 100 to infuse the porous Teflon membrane with an average pore size of 200 nm. The perfluorinated liquid is used because it is immiscible in both the aqueous and nonaqueous phases due to the extremely low surface tension. After spraying onto the porous Teflon surface, the perfluorinated fluid droplet quickly wicks into the pores and wets the membrane. To determine the changes in roughness and surface properties of the Teflon surface before and after introduction of the perfluorinated liquid coating, a sessile

DOI: 10.1021/acsami.6b16141
ACS Appl. Mater. Interfaces 2017, 9, 7472−7480

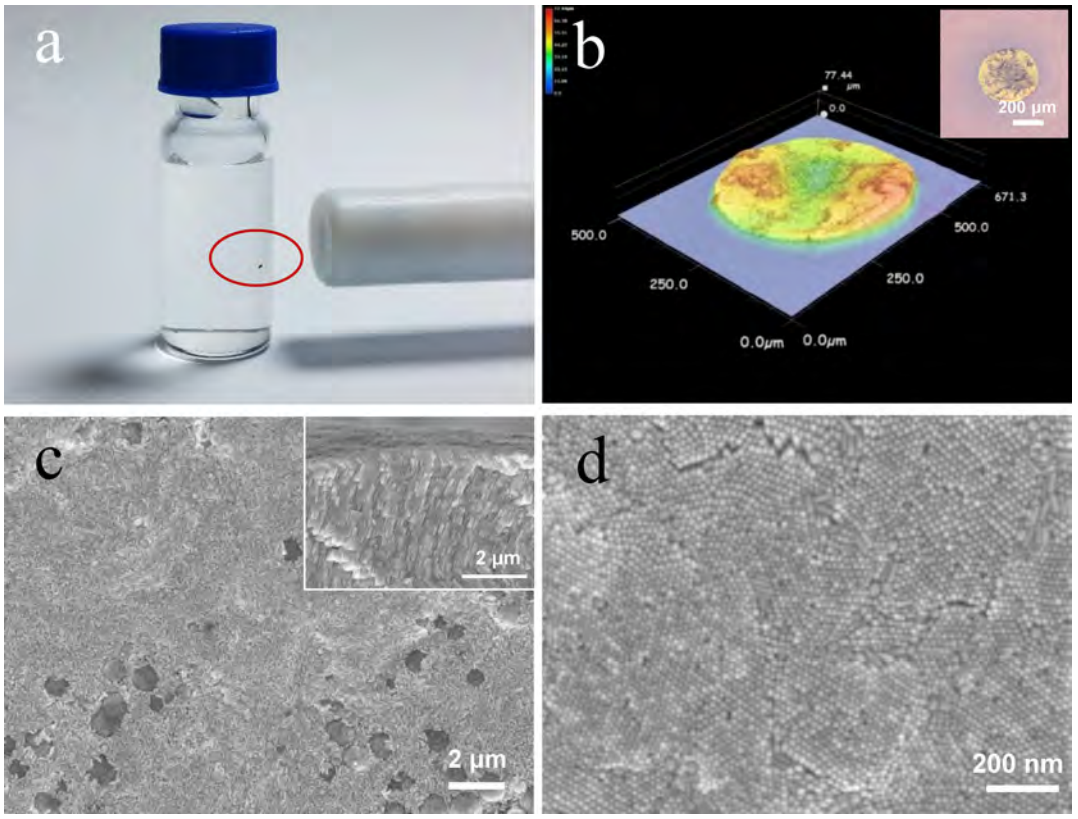

Figure 3. (a) Photograph of the AuNRs array doped with Fe_3O_4 NPs in water; (b) Confocal laser scattering microscopic 3D image with the inset photograph; (c, d) SEM images with different views of the array.

droplet of the AuNRs suspension (20 μL) is dripped on the surface of both the treated and untreated Teflon membranes. Figure 1b shows the slippery performance by titling at a very small angle. When the titling angle is increased to 4°, the droplet slides on the treated lubricated Teflon membrane but it remains on the untreated membrane due to the pinning effect. As the nanotexture of the Teflon membrane is impregnated with the perfluorinated liquid, the sharp edges are smoothed by the liquid lubricant yielding a lubricated rough surface.[24] The pinning effect on the surface is thus reduced and droplet mobility can be retained regardless of the droplet wetting states, i.e. Cassie–Baxter state[25] and Wenzel state.[26] The mobility of the sessile droplet on the lubricated Teflon surface can induce three-phase contact line sliding of the droplet during evaporation and droplet condensation.[27] It provides the desirable platform for enrichment and clustering of NPs.

Figure 2 shows the morphology of the AuNRs and Fe_3O_4 NPs to be used in the subsequent evaporative self-assembly experiments. The MUDOL-coated AuNRs (labeled MUDOL-AuNRs) are obtained by a technique reported by our group previously.[20] In brief, the CTAB coated AuNRs (CTAB-AuNRs) are synthesized by a seed-mediated method and the surface ligands on the AuNRs are exchanged with MUDOL, a commercially available amphiphilic PEGylated alkanethiolate ligand bearing a thiol moiety. The FTIR spectra in Supporting Information (SI) Figure S1a demonstrate successful ligand exchange from CTAB to MUDOL. It has been demonstrated that ligand exchange can induce side-to-side assembly of the AuNRs,[28] which can be confirmed by the blue-shift in the longitudinal surface plasmon resonance (SPR) of the AuNRs (see SI Figure S1b) and the TEM image in Figure 2a. In comparison, the Fe_3O_4 NPs are synthesized by a general solvent-thermal method[29] and the spherical morphology of the Fe_3O_4 NPs is revealed by the SEM image in Figure 2b.

The concentrated AuNRs suspension is mixed Fe_3O_4 suspension to form the hybrid NPs suspension and no aggregation is noticed. The droplet of AuNRs and Fe_3O_4 hybrid NPs is evaporated on the slippery platform and droplet condensation and NPs enrichment are shown in Figure 2c. The AuNRs with the MUDOL coating produce the side-to-side packing behavior and Marangoni flow inside the droplet.[30] As the droplet is evaporated, the MUDOL-AuNRs are side-to-side assembled with Fe_3O_4 NPs mingled inside the assembly. The MUDOL molecules in the droplet also contribute to the Marangoni flow and inward flow induced by the gradient in the surface tension along the liquid–gas interface.[31] The coffee-ring effect is thus suppressed and the hybrid NPs are pushed away from the contact line and redistributed back to the central droplet region leading to uniform deposition. Meanwhile, the pinning effect is nearly eliminated on this slippery platform. The three-phase contact line keeps sliding inward resulting in decrease in the droplet volume during evaporation until completion. The hybrid NPs inside the droplet are self-assembled and enriched as the droplet condenses.

Figure 2d shows the drying process of a 40 μL droplet on the liquid lubricant Teflon membrane. The volume of the droplet decreases gradually, and after 6 h evaporation an array that can be detached from the Teflon membrane is formed. The MUDOL-AuNRs form the regular packing area and the Fe_3O_4 NPs endow it with magnetic properties. Figure 2e shows the batch fabrication of the arrays and states of 50, 40, 30, 20, and 10 μL droplets before and after drying. All the droplets are finally dried forming arrays and as the volume decreases, the diameter of the arrays decreases correspondingly from 0.95 mm

DOI: 10.1021/acsami.6b16141
ACS Appl. Mater. Interfaces 2017, 9, 7472–7480

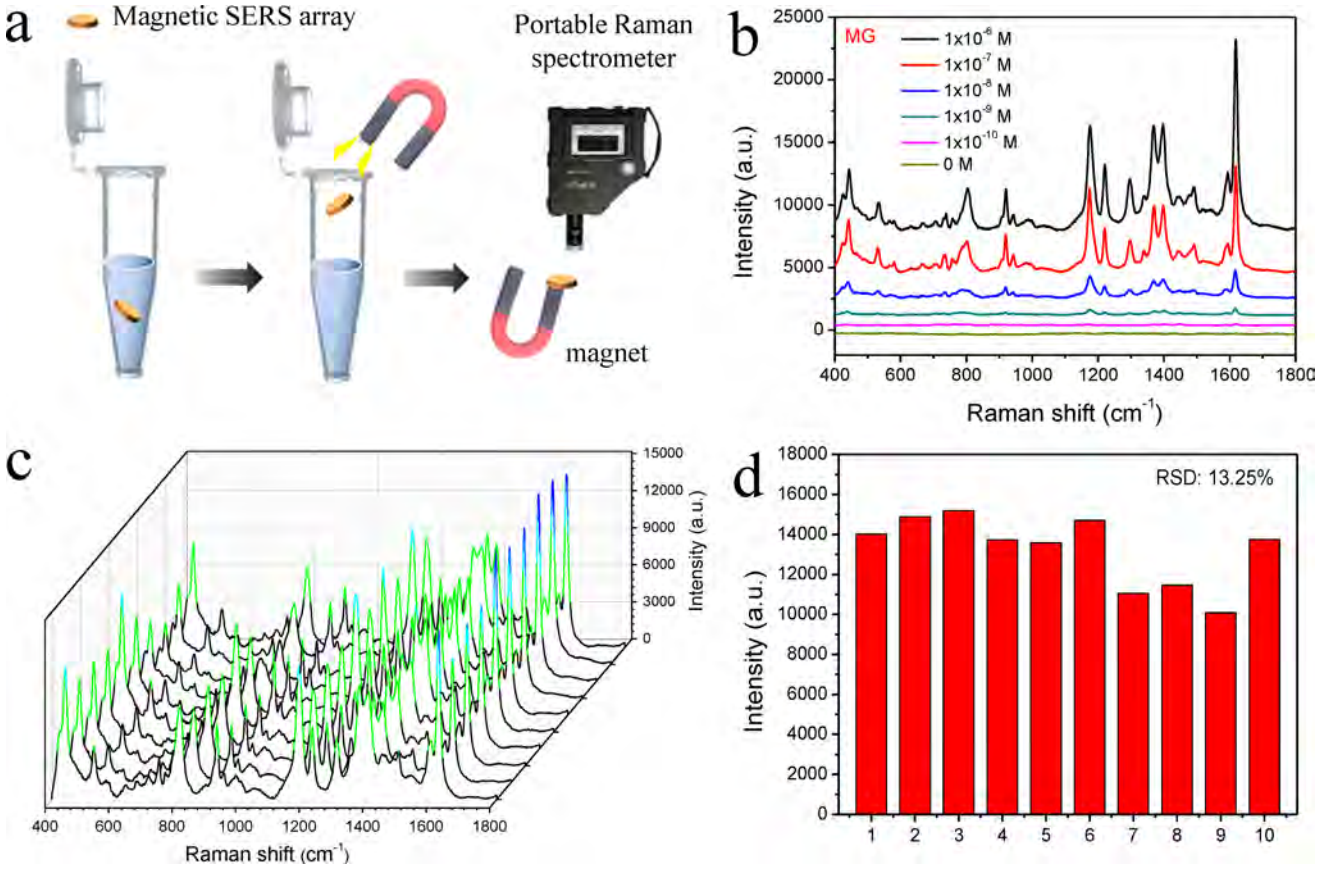

Figure 4. (a) Schematic illustration of the magnetic separation and detection processes with the removable array as the SERS substrate; (b) SERS spectra (λ_{ex} = 633 nm) for different concentrations (1×10^{-6} to 1×10^{-10} M) of MG; (c, d) SERS spectra of MG acquired from 10 different spots on a single substrate and corresponding histogram for the peak intensity at 1615 cm^{-1}.

(50 μL) to 0.4 mm (10 μL). For the fabrication of the substrate, a little amount of the hybrid NPs suspension is needed, thus this droplet evaporation method is excellent for the batch fabrication of the substrate.

Figure 3a shows a typical array detached from the membrane and put in a water solution. No disassembly of the array is observed and the movement response to a magnetic bar confirms the magnetic characteristics. The morphology and structure of the array are characterized by confocal laser scattering microscopy and SEM (see Figure 3b–d). The SERS array shows a 3D morphology with a diameter of 0.55 mm and height of 65 μm together with a relatively flat surface due to elimination of the coffee-ring effect. The SEM image discloses dense and vertically aligned self-assembled AuNRs, and some Fe_3O_4 NPs are randomly and closely embedded in the array. With increasing amount of Fe_3O_4 NPs in the hybrid NPs, more Fe_3O_4 NPs are observed on the array surface (SI Figure S2), but the AuNRs superlattice structure is not significantly affected. The cross-sectional SEM image in the inset in Figure 3c confirms that the ordered AuNRs structure consists of tens of layers of densely packed standing AuNRs. Figure 3d highlights a local area without the Fe_3O_4 NPs and the AuNRs are dense, regular, and nearly vertically aligned with respect to the surface. The results demonstrate successful fabrication of the 3D AuNRs plasmonic superlattice array doped with Fe_3O_4 NPs. The introduction of magnetic nanoparticles into SERS substrates has been previously reported, but only in terms of nanoscale composites.[32−35] Here, macroscale 3D plasmonic superlattice arrays are obtained and can be used as a novel magnetic SERS substrate.

It is a green and straightforward method to prepare a macroscale superlattice array of hybrid NPs. The liquid infused porous slippery surface inspired by the *Nepenthes* pitcher plant[36] is introduced as the base materials for self-assembly of NPs. The slippery surface acts as a pinning-free platform to enrich NPs due to inward contact line sliding during droplet evaporation as a result of the low surface energy substrate and low surface tension liquid.[37] MUDOL modification of the AuNRs not only enables side-to-side assembly of the AuNRs, but also suppresses the outward capillary flow as well as coffee-ring effect, resulting in uniform and dense assembly of the AuNRs doped with Fe_3O_4 NPs. The array formed by this method is of interest from three perspectives. First, the NPs and Teflon membrane are separated by the perfluorinated liquid during evaporation. The array as a whole does not make direct contact with the Teflon membrane and therefore, it can be easily detached from the membrane. Second, it can be easily manipulated by a magnetic field without clustering decrease, which is a common problem for many magnetic particles. The magnetic Fe_3O_4 NPs are enclosed in the AuNRs arrays to minimize leaching. The third feature is that the 3D superlattice array is composed of dense, regular, and vertically aligned AuNRs. The 3D organization of AuNRs into macroscopic superlattices leads to an excellent plasmonic substrate.

A typical array comprising AuNRs and Fe_3O_4 NPs with a diameter of about 0.55 mm is adopted as a magnetic SERS substrate. As shown in Figure 4a, the concept of manipulation is

DOI: 10.1021/acsami.6b16141
ACS Appl. Mater. Interfaces 2017, 9, 7472−7480

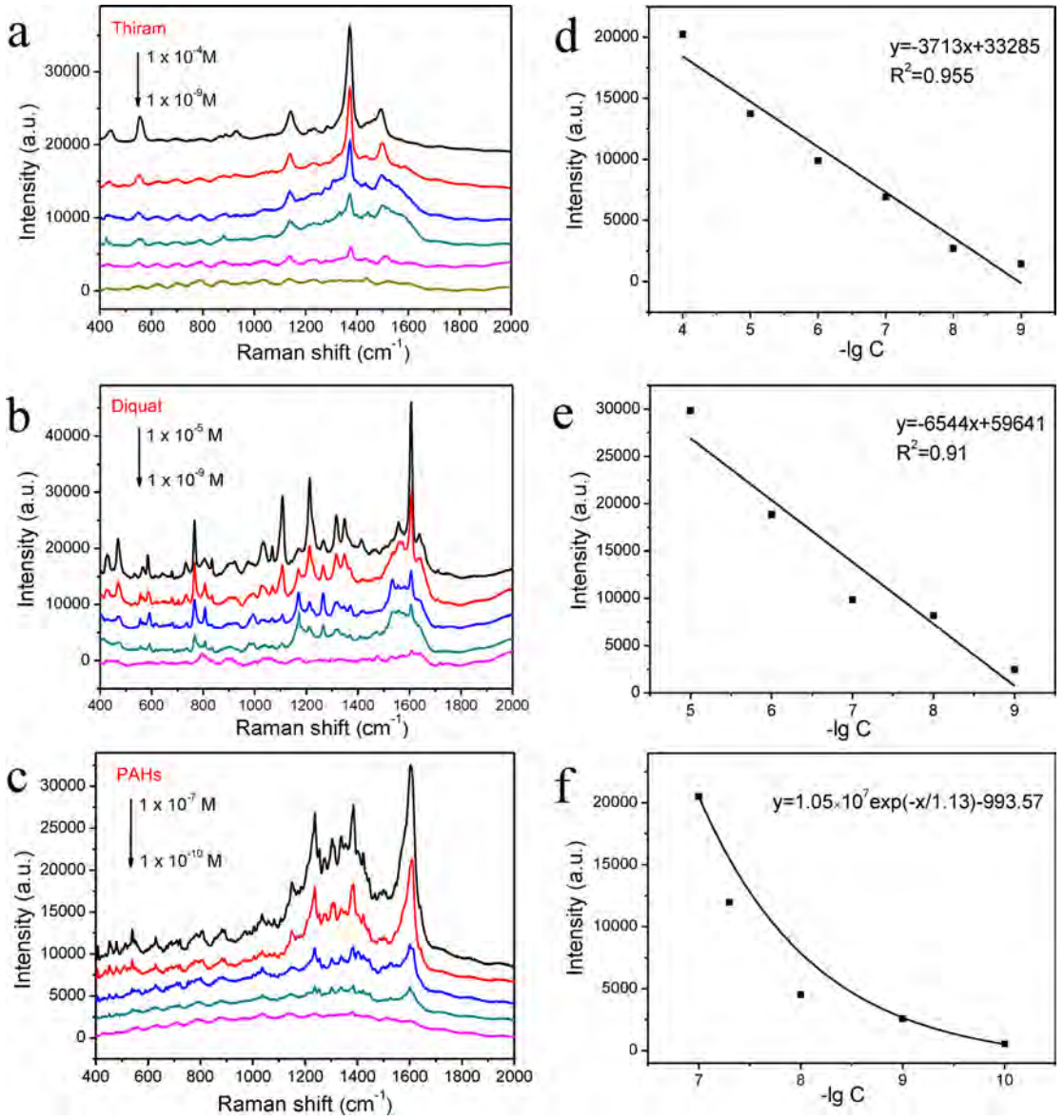

Figure 5. SERS spectra (λ_{ex} = 633 nm) and corresponding intensity-concentration relationship extracted from the strongest peak of different concentrations: (a, d) thiram, (b, e) diquat, and (c, f) PAHs.

to soak the magnetic SERS substrate in the solution in order to achieve abundant capturing of analyte molecules. The substrate with the analyte molecules is separated from the solution with the aid of a magnet and SERS can be implemented after the substrate is dried. The drying process of the substrate collected from the analytes solution lasts about 10 min, and the SERS signal acquisition time for each test spot is 10 s. The SERS performance of the magnetic SERS substrate is evaluated with the banned fish pesticide malachite green (MG) on a portable Raman scattering instrument with 633 nm excitation. The SERS spectra for different concentrations of MG from 1.0×10^{-6} to 1.0×10^{-10} M are shown in Figure 4b. The spectrum of the blank substrate (0 M) confirms that CTAB and MUDOL molecules have no interferences on the detection. The characteristic Raman peaks of MG are revealed, for example, ring C−C stretching (1615 cm^{-1}), *N*-phenyl stretching (1397 cm^{-1}), ring C−H in-plane bending (1172 cm^{-1}), C−H out-of-plane bending (917 and 798 cm^{-1}), and phenyl−C−phenyl out-of-plane bending (438 cm^{-1}).[38] The peaks can be detected even at a concentration down to 1.0×10^{-10} M, indicating that the detection limit is lower than the technique limit (2.0 $\mu g\ L^{-1}$) for MG. The reproducibility is also investigated with a 1.0×10^{-6} M MG solution and the spectra obtained from 10 randomly selected spots are displayed in Figure 4c. The magnetic substrate with optimized amount of Fe_3O_4 NPs is used in the SERS detection. The SERS active areas on the AuNRs superlattices are not affect by the Fe_3O_4 NPs, so the relatively consistent signal intensity of each characteristic band of MG is observed. The spot-to-spot variation of the SERS intensity for the 1615 cm^{-1} peak from the 10 spots is analyzed and the relative standard deviation (RSD) is calculated to be 13.25% (Figure 4d). The SERS mapping of MG with a randomly chosen 30 μm × 30 μm area exhibited in SI Figure S3 also indicates the reasonable overall reproducibility (RSD: 25.6%) of the SERS substrate. The results demonstrate that the removable and magnetic SERS substrate has good reliability.

The magnetic-separation SERS technique is employed to detect three typical environmental pollutants, namely thiram,

DOI: 10.1021/acsami.6b16141
ACS Appl. Mater. Interfaces 2017, 9, 7472−7480

diquat, and polycyclic aromatic hydrocarbons (PAHs). Thiram and diquat are common residues in soil and highly toxic producing diseases. Figure 5a shows the typical SERS spectra of thiram at different concentrations. They are dominated by the CH_3 stretching mode at 1495 cm^{-1}, CN stretching mode at 1372 cm^{-1}, as well as SS stretching mode at 556 cm^{-1}.[39] The strongest peak at 1372 cm^{-1} can be used in quantitative analysis. Figure 5d shows the linear relationship between the peak intensity and negative logarithm of the thiram concentration. A good linear relationship with the square of linear correlation coefficient (R^2) of 0.955 is observed indicative of accurate quantitative evaluation of thiram. The detection limit is 1×10^{-9} M which is much lower than the maximal residue limit of 7 ppm in fruits as specified by the U.S. Environmental Protection Agency (EPA).[40] With regard to diquat detection, the main Raman peaks at 765 cm^{-1} (in plane deformation), 1213 cm^{-1} (wagging of $-CH_2$), and 1606 cm^{-1} (symmetric ring stretching vibrations) are observed and the strongest one at 1606 cm^{-1} is selected in the quantitative evaluation.[41,42] The detection limit is 1×10^{-9} M (see Figure 5b) and a good linear relationship between the negative logarithm of concentration and peak intensity with R^2 of 0.91 is demonstrated in Figure 5e.

PAHs are a class of permanent organic pollutants requiring complex pretreatment in traditional analysis. The removable substrate here can mitigate the difficulty in sample preparation and provide rapid analysis. The solutions of standard sample containing 16 PAHs at different concentrations are detected with this substrate. As shown in Figure 5c, the three main Raman peaks at 1236, 1385, and 1605 cm^{-1} correspond to the in-plane ring-stretch vibration of composite signals from individual molecules in the PAHs.[43] Although the key SERS peaks of the individual peaks overlap making them difficult to distinguish, the detection of the mix solution is still of great importance because PAHs always exhibit in terms of mixtures in practical samples. Nonetheless, the detection limit of PAHs is 1×10^{-10} M and there is a good exponential relationship between the peak intensity at 1605 cm^{-1} and negative logarithm of concentration (see Figure 5f), implying that the technique is applicable to the quantitative analysis of PAHs solutions. The calibration curve of PAHs is different from the linear relationship ones of thiram and diquat. The main reason is that solution of PAHs is a mixture solution consist of 16 different polycyclic aromatic hydrocarbons molecules. The characteristic peaks arise from the particular functional groups in different molecules, but the intensities are not simply the add-up of those from different molecules, so the intensities at different concentrations are not linear related to the negative logarithm of concentrations. These satisfactory detection results of the standard samples of three environmental pollutants imply the possibility of the detection of the real environmental samples. However, the work of real sample detection is a systematic study, requiring complex pretreatment and abundant data collection, and it will be carried out in future work.

4. CONCLUSIONS

In conclusion, macroscale AuNRs superlattice arrays doped with Fe_3O_4 NPs have been successfully fabricated by the efficient enrichment and self-assembly of the hybrid nanoparticles for SERS detection of environmental pollutants. A slippery platform comprising a low surface energy substrate and low surface tension liquid endows with the pinning-free enrichment of the droplet and MUDOL molecules facilitate the regular self-assembly of AuNRs. The obtained arrays not only present a dense and regular plasmonic superlattice structure, but also possess magnetic properties enabling rapid separation of analytes from the solution in SERS detection. The magnetic-separation SERS strategy enables rapid detection of three environmental pollutants with sensitivity down to the nanomolar level. The results indicate that this removable and magnetic array can be an efficient SERS substrate for various detection applications. Moreover, this self-assembly method can be readily extended to the preparation of removable superlattice arrays with different nanoparticles.

■ ASSOCIATED CONTENT

Supporting Information

The Supporting Information is available free of charge on the ACS Publications website at DOI: 10.1021/acsami.6b16141.

FTIR spectra and adsorption spectra of CTAB-AuNRs and MUDOL-AuNRs. SEM images of the SERS array. SERS mapping of MG from the SERS array (PDF)

■ AUTHOR INFORMATION

Corresponding Authors

*(P.H.L.) E-mail: ph.li@siat.ac.cn.
*(Q. L.) E-mail: qian.luo@siat.ac.cn.
*(X.-F.Y.) Phone: 86-755-86392212; fax: 86-755-86585222; e-mail: xf.yu@siat.ac.cn.

ORCID

Xue-Feng Yu: 0000-0003-2566-6194

Author Contributions

‖These authors contributed equally. All authors have given approval to the final version of the manuscript.

Notes

The authors declare no competing financial interest.

■ ACKNOWLEDGMENTS

This work was jointly supported by the National Natural Science Fund of China Nos. 51372175, 91543105, Shenzhen Science and Technology Research Funding Nos. CXZZ20150813160047997, JCYJ20120615124830232, JSGG20160229204218661, the Key Laboratory of Optoelectronic Devices and Systems of Ministry of Education and Guangdong Province (GD201607), the Program of Public Interest Research and Capability Construction of Guangdong Province (2014A010105034), Hong Kong Research Grants Council (RGC) General Research Funds (GRF) No. 11301215, and SIAT-Gran-Biological Joint Laboratory.

■ REFERENCES

(1) Nie, S.; Emory, S. R. Probing Single Molecules and Single Nanoparticles by Surface-Enhanced Raman Scattering. *Science* **1997**, *275*, 1102−1106.
(2) Si, K. J.; Guo, P.; Shi, Q.; Cheng, W. Self-Assembled Nanocube-Based Plasmene Nanosheets as Soft Surface-Enhanced Raman Scattering Substrates Toward Direct Quantitative Drug Identification on Surfaces. *Anal. Chem.* **2015**, *87*, 5263−5269.
(3) Zhu, C.; Meng, G.; Zheng, P.; Huang, Q.; Li, Z.; Hu, X.; Wang, X.; Huang, Z.; Li, F.; Wu, N. A Hierarchically Ordered Array of Silver-Nanorod Bundles for Surface-Enhanced Raman Scattering Detection of Phenolic Pollutants. *Adv. Mater.* **2016**, *28*, 4871−4876.
(4) Xiao, X.; Yan, K.; Xu, X.; Li, G. Rapid Analysis of Ractopamine in Pig Samples by Dummy-Template Imprinted Solid-Phase Extraction

DOI: 10.1021/acsami.6b16141
ACS Appl. Mater. Interfaces 2017, 9, 7472−7480

Coupling with Surface-Enhanced Raman Spectroscopy. *Talanta* **2015**, *138*, 40−45.
(5) Pazos, E.; Garcia-Algar, M.; Penas, C.; Nazarenus, M.; Torruella, A.; Pazos-Perez, N.; Guerrini, L.; Vázquez, M. E.; Garcia-Rico, E.; Mascareñas, J. L.; Alvarez-Puebla, R. A. Surface-Enhanced Raman Scattering Surface Selection Rules for the Proteomic Liquid Biopsy in Real Samples: Efficient Detection of the Oncoprotein c-MYC. *J. Am. Chem. Soc.* **2016**, *138*, 14206−14209.
(6) Zhang, X.; Zheng, Y.; Liu, X.; Lu, W.; Dai, J.; Lei, D. Y.; MacFarlane, D. R. Hierarchical Porous Plasmonic Metamaterials for Reproducible Ultrasensitive Surface-Enhanced Raman Spectroscopy. *Adv. Mater.* **2015**, *27*, 1090−1096.
(7) Kanipe, K. N.; Chidester, P. P. F.; Stucky, G. D.; Moskovits, M. Large Format Surface-Enhanced Raman Spectroscopy Substrate Optimized for Enhancement and Uniformity. *ACS Nano* **2016**, *10*, 7566−7571.
(8) Lee, J.; Zhang, Q.; Park, S.; Choe, A.; Fan, Z.; Ko, H. Particle-Film Plasmons on Periodic Silver Film over Nanosphere (AgFON): A Hybrid Plasmonic Nanoarchitecture for Surface-Enhanced Raman Spectroscopy. *ACS Appl. Mater. Interfaces* **2016**, *8*, 634−642.
(9) Jeong, J. W.; Arnob, M. M. P.; Baek, K.-M.; Lee, S. Y.; Shih, W.-C.; Jung, Y. S. 3D Cross-Point Plasmonic Nanoarchitectures Containing Dense and Regular Hot Spots for Surface-Enhanced Raman Spectroscopy Analysis. *Adv. Mater.* **2016**, *28*, 8695−8704.
(10) Gómez-Graña, S.; Pérez-Juste, J.; Alvarez-Puebla, R. A.; Guerrero-Martínez, A.; Liz-Marzán, L. M. Self-Assembly of Au@Ag Nanorods Mediated by Gemini Surfactants for Highly Efficient SERS-Active Supercrystals. *Adv. Opt. Mater.* **2013**, *1*, 477−481.
(11) Barrow, S. J.; Wei, X.; Baldauf, J. S.; Funston, A. M.; Mulvaney, P. The Surface Plasmon Modes of Self-Assembled Gold Nanocrystals. *Nat. Commun.* **2012**, *3*, 1275.
(12) Boles, M. A.; Engel, M.; Talapin, D. V. Self-Assembly of Colloidal Nanocrystals: From Intricate Structures to Functional Materials. *Chem. Rev.* **2016**, *116*, 11220−11289.
(13) Wang, P.-Y.; Shields, C. W.; Zhao, T.; Jami, H.; López, G. P.; Kingshott, P. Rapid Self-Assembly of Shaped Microtiles into Large, Close-Packed Crystalline Monolayers on Solid Surfaces. *Small* **2016**, *12*, 1309−1314.
(14) Ming, T.; Kou, X.; Chen, H.; Wang, T.; Tam, H.-L.; Cheah, K.-W.; Chen, J.-Y.; Wang, J. Ordered Gold Nanostructure Assemblies Formed By Droplet Evaporation. *Angew. Chem., Int. Ed.* **2008**, *47*, 9685−9690.
(15) Chen, H.; Shao, L.; Li, Q.; Wang, J. Gold Nanorods and Their Plasmonic Properties. *Chem. Soc. Rev.* **2013**, *42*, 2679−2724.
(16) Talbot, E. L.; Yang, L.; Berson, A.; Bain, C. D. Control of the Particle Distribution in Inkjet Printing through an Evaporation-Driven Sol−Gel Transition. *ACS Appl. Mater. Interfaces* **2014**, *6*, 9572−9583.
(17) Li, Y.; Lv, C.; Li, Z.; Quéré, D.; Zheng, Q. From Coffee Rings to Coffee Eyes. *Soft Matter* **2015**, *11*, 4669−4673.
(18) Still, T.; Yunker, P. J.; Yodh, A. G. Surfactant-Induced Marangoni Eddies Alter the Coffee-Rings of Evaporating Colloidal Drops. *Langmuir* **2012**, *28*, 4984−4988.
(19) Sempels, W.; De Dier, R.; Mizuno, H.; Hofkens, J.; Vermant, J. Auto-Production of Biosurfactants Reverses the Coffee Ring Effect in A Bacterial System. *Nat. Commun.* **2013**, *4*, 1757.
(20) Li, P.; Li, Y.; Zhou, Z.-K.; Tang, S.; Yu, X.-F.; Xiao, S.; Wu, Z.; Xiao, Q.; Zhao, Y.; Wang, H.; Chu, P. K. Evaporative Self-Assembly of Gold Nanorods into Macroscopic 3D Plasmonic Superlattice Arrays. *Adv. Mater.* **2016**, *28*, 2511−2517.
(21) Jin, H.; Qian, J.; Zhou, L.; Yuan, J.; Huang, H.; Wang, Y.; Tang, W. M.; Chan, H. L. W. Suppressing the Coffee-Ring Effect in Semitransparent MnO_2 Film for a High-Performance Solar-Powered Energy Storage Window. *ACS Appl. Mater. Interfaces* **2016**, *8*, 9088−9096.
(22) Kuang, M.; Wang, L.; Song, Y. Controllable Printing Droplets for High-Resolution Patterns. *Adv. Mater.* **2014**, *26*, 6950−6958.
(23) Jiang, C.; Zhong, Z.; Liu, B.; He, Z.; Zou, J.; Wang, L.; Wang, J.; Peng, J. B.; Cao, Y. Coffee-Ring-Free Quantum Dot Thin Film Using Inkjet Printing from a Mixed-Solvent System on Modified ZnO Transport Layer for Light-Emitting Devices. *ACS Appl. Mater. Interfaces* **2016**, *8*, 26162−26168.
(24) Dai, X.; Stogin, B. B.; Yang, S.; Wong, T.-S. Slippery Wenzel State. *ACS Nano* **2015**, *9*, 9260−9267.
(25) Cassie, A. B. D.; Baxter, S. Wettability of Porous Surfaces. *Trans. Faraday Soc.* **1944**, *40*, 546−551.
(26) Wenzel, R. N. Resistance of Solid Surfaces to Wetting by Water. *Ind. Eng. Chem.* **1936**, *28*, 988−994.
(27) Guan, J. H.; Wells, G. G.; Xu, B.; McHale, G.; Wood, D.; Martin, J.; Stuart-Cole, S. Evaporation of Sessile Droplets on Slippery Liquid-Infused Porous Surfaces (SLIPS). *Langmuir* **2015**, *31*, 11781−11789.
(28) Xie, Y.; Guo, S.; Ji, Y.; Guo, C.; Liu, X.; Chen, Z.; Wu, X.; Liu, Q. Self-Assembly of Gold Nanorods into Symmetric Superlattices Directed by OH-Terminated Hexa(ethylene glycol) Alkanethiol. *Langmuir* **2011**, *27*, 11394−11400.
(29) Wang, L.; Li, J.; Jiang, Q.; Zhao, L. Water-Soluble Fe_3O_4 Nanoparticles with High Solubility for Removal of Heavy-Metal Ions from Waste Water. *Dalton Trans.* **2012**, *41*, 4544−4551.
(30) Hamon, C.; Novikov, S.; Scarabelli, L.; Basabe-Desmonts, L.; Liz-Marzán, L. M. Hierarchical Self-Assembly of Gold Nanoparticles into Patterned Plasmonic Nanostructures. *ACS Nano* **2014**, *8*, 10694−10703.
(31) Anyfantakis, M.; Geng, Z.; Morel, M.; Rudiuk, S.; Baigl, D. Modulation of the Coffee-Ring Effect in Particle/Surfactant Mixtures: the Importance of Particle-Interface Interactions. *Langmuir* **2015**, *31*, 4113−4120.
(32) Kim, K.; Choi, J.-Y.; Lee, H. B.; Shin, K. S. Silanization of Ag-Deposited Magnetite Particles: An Efficient Route to Fabricate Magnetic Nanoparticle-Based Raman Barcode Materials. *ACS Appl. Mater. Interfaces* **2010**, *2*, 1872−1878.
(33) Spuch-Calvar, M.; Rodríguez-Lorenzo, L.; Morales, M. P.; Álvarez-Puebla, R. A.; Liz-Marzán, L. M. Bifunctional Nanocomposites with Long-Term Stability as SERS Optical Accumulators for Ultrasensitive Analysis. *J. Phys. Chem. C* **2009**, *113*, 3373−3377.
(34) Contreras-Cáceres, R.; Abalde-Cela, S.; Guardia-Girós, P.; Fernández-Barbero, A.; Pérez-Juste, J.; Alvarez-Puebla, R. A.; Liz-Marzán, L. M. Multifunctional Microgel Magnetic/Optical Traps for SERS Ultradetection. *Langmuir* **2011**, *27*, 4520−4525.
(35) Zhou, X.; Xu, W.; Wang, Y.; Kuang, Q.; Shi, Y.; Zhong, L.; Zhang, Q. Fabrication of Cluster/Shell Fe_3O_4/Au Nanoparticles and Application in Protein Detection via a SERS Method. *J. Phys. Chem. C* **2010**, *114*, 19607−19613.
(36) Wong, T.-S.; Kang, S. H.; Tang, S. K. Y.; Smythe, E. J.; Hatton, B. D.; Grinthal, A.; Aizenberg, J. Bioinspired Self-Repairing Slippery Surfaces with Pressure-Stable Omniphobicity. *Nature* **2011**, *477*, 443−447.
(37) Yang, S.; Dai, X.; Stogin, B. B.; Wong, T.-S. Ultrasensitive Surface-Enhanced Raman Scattering Detection in Common Fluids. *Proc. Natl. Acad. Sci. U. S. A.* **2016**, *113*, 268−273.
(38) Shao, J.; Tong, L.; Tang, S.; Guo, Z.; Zhang, H.; Li, P.; Wang, H.; Du, C.; Yu, X.-F. PLLA Nanofibrous Paper-Based Plasmonic Substrate with Tailored Hydrophilicity for Focusing SERS Detection. *ACS Appl. Mater. Interfaces* **2015**, *7*, 5391−5399.
(39) Saute, B.; Narayanan, R. Solution-Based Direct Readout Surface Enhanced Raman Spectroscopic (SERS) Detection of Ultra-Low Levels of Thiram with Dogbone Shaped Gold Nanoparticles. *Analyst* **2011**, *136*, 527−532.
(40) Zhang, L.; Jiang, C.; Zhang, Z. Graphene Oxide Embedded Sandwich Nanostructures for Enhanced Raman Readout and Their Applications in Pesticide Monitoring. *Nanoscale* **2013**, *5*, 3773−3779.
(41) Lopez-Ramirez, M. R.; Guerrini, L.; Garcia-Ramos, J. V.; Sanchez-Cortes, S. Vibrational Analysis of Herbicide Diquat: A Normal Raman and SERS Study on Ag Nanoparticles. *Vib. Spectrosc.* **2008**, *48*, 58−64.
(42) Roldán, M. L.; Sanchez-Cortes, S.; García-Ramos, J. V.; Domingo, C. Cucurbit[8]uril-Stabilized Charge Transfer Complexes with Diquat Driven by pH: A SERS Study. *Phys. Chem. Chem. Phys.* **2012**, *14*, 4935−4941.

DOI: 10.1021/acsami.6b16141
ACS Appl. Mater. Interfaces 2017, 9, 7472−7480

(43) Du, J.; Xu, J.; Sun, Z.; Jing, C. Au Nanoparticles Grafted on Fe_3O_4 as Effective SERS Substrates for Label-Free Detection of the 16 EPA Priority Polycyclic Aromatic Hydrocarbons. *Anal. Chim. Acta* **2016**, *915*, 81−89.

DOI: 10.1021/acsami.6b16141
ACS Appl. Mater. Interfaces 2017, 9, 7472−7480

Supporting Information

Efficient Enrichment and Self-Assembly of Hybrid Nanoparticles into Removable and Magnetic SERS Substrates for Sensitive Detection of Environmental Pollutants

Siying Tang,[†,∥] Yong Li,[†,∥] Hao Huang,[†] Penghui Li,[*,†,‡] Zhinan Guo,[†,§] Qian Luo,[*,†] Zhe Wang,[†] Paul K. Chu,[‡] Jia Li,[†] and Xue-Feng Yu[*,†]

[†]Institute of Biomedicine and Biotechnology, Shenzhen Institutes of Advanced Technology, Chinese Academy of Sciences, Shenzhen 518055, P. R. China

[‡]Department of Physics and Materials Science, City University of Hong Kong, Tat Chee Avenue, Kowloon, Hong Kong, P. R. China

[§]SZU-NUS Collaborative Innovation Center for Optoelectronic Science and Technology, and Key Laboratory of Optoelectronic Devices and Systems of Ministry of Education and Guangdong Province, College of Optoelectronic Engineering, Shenzhen University, Shenzhen 518060, P.R. China

Corresponding Authors:

*(P.H.L.) E-mail: ph.li@siat.ac.cn.

*(Q.L.) E-mail: qian.luo@siat.ac.cn.

*(X.-F.Y.) Phone: 86-755-86392212; fax: 86-755-86585222; e-mail: xf.yu@siat.ac.cn.

The FTIR and adsorption spectra of AuNRs acquired before and after the surface ligand exchange are recorded and shown in Figure S1a. The new intense band at 1100 cm^{-1} arising from C–O–C stretching in ethylene glycol moieties and broad peak around 3345 cm^{-1} assigned to the -OH groups in the MUDOL molecule in the FTIR spectrum of MUDOL-AuNRs confirm successful binding of MUDOL molecules onto the AuNRs surface. As shown in Figure S1b, the significant blue-shift in the longitudinal SPR band indicates side-to-side assembly of the AuNRs after ligand exchange.

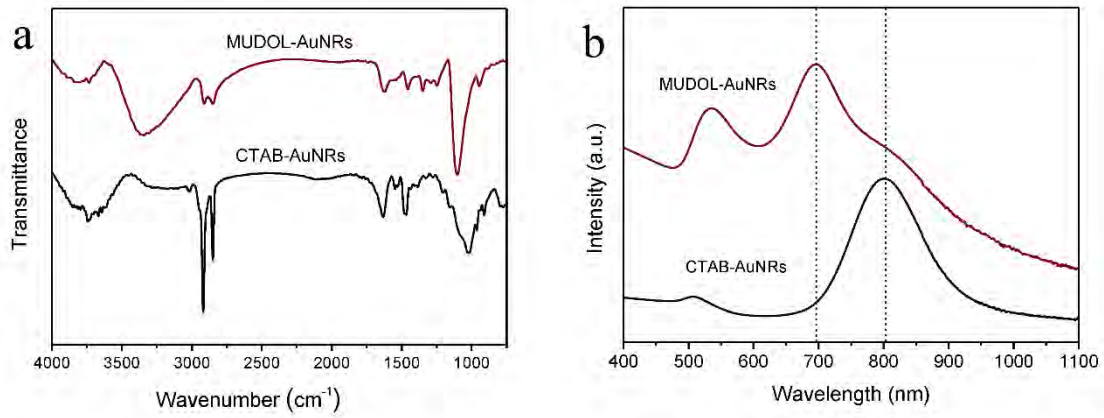

Figure S1. (a) FTIR spectra and (b) adsorption spectra of CTAB-AuNRs and MUDOL-AuNRs.

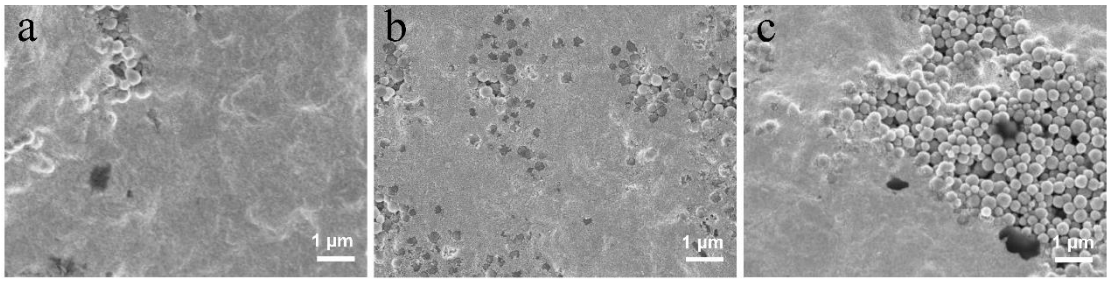

Figure S2. SEM images of SERS arrays with different relative amount ratios of AuNRs and Fe_3O_4 NPs: (a) 1000: 1, (b) 500: 1, and (c) 100: 1.

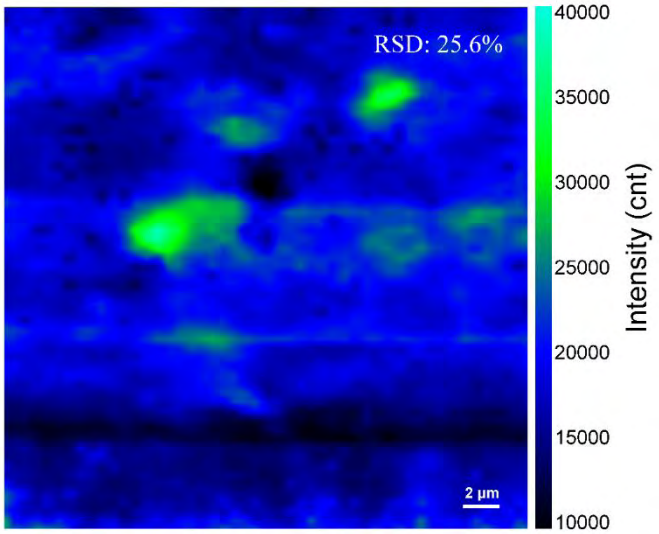

Figure S3. SERS mapping of a 30 μm × 30 μm area in the array by point-by-point scanning mode using a step size of 0.5 μm upon laser excitation against MG with concentration of 1×10^{-6} M.